Indistinguishability-based quantum coherence: activation, particle statistics imprint and enhanced metrological applications

Kai Sun[a,b,1], **Zheng-Hao Liu**[a,b,1], **Yan Wang**[a,b], **Ze-Yan Hao**[a,b], **Xiao-Ye Xu**[a,b], **Jin-Shi Xu**[a,b,2], **Chuan-Feng Li**[a,b,2], **Guang-Can Guo**[a,b], **Alessia Castellini**[c], **Ludovico Lami**[d], **Andreas Winter**[e], **Gerardo Adesso**[f], **Giuseppe Compagno**[c], and **Rosario Lo Franco**[g,2]

[a]CAS Key Laboratory of Quantum Information, University of Science and Technology of China, Hefei 230026, People's Republic of China; [b]CAS Centre For Excellence in Quantum Information and Quantum Physics, University of Science and Technology of China, Hefei 230026, People's Republic of China; [c]Dipartimento di Fisica e Chimica - Emilio Segrè, Università di Palermo, via Archirafi 36, 90123 Palermo, Italy; [d]Institut für Theoretische Physik und IQST, Universität Ulm, Albert-Einstein-Allee 11, D-89069 Ulm, Germany; [e]ICREA & Física Teórica: Informació i Fenómens Quàntics, Departament de Física, Universitat Autònoma de Barcelona, ES-08193 Bellaterra (Barcelona), Spain; [f]School of Mathematical Sciences and Centre for the Mathematics and Theoretical Physics of Quantum Non-Equilibrium Systems, University of Nottingham, University Park, Nottingham NG/ 2RD, United Kingdom; [g]Dipartimento di Ingegneria, Università di Palermo, Viale delle Scienze, Edificio 6, 90128 Palermo, Italy

This manuscript was compiled on March 30, 2022

Quantum coherence, an essential feature of quantum mechanics allowing superpositions of quantum states, is a resource for quantum information processing. Coherence emerges in a fundamentally different way for nonidentical and identical particles. For the latter, a unique contribution exists linked to indistinguishability that cannot occur for nonidentical particles. Here, we experimentally demonstrate this additional contribution to quantum coherence with an optical setup, showing its amount directly depends on the degree of indistinguishability and exploiting it in a quantum phase discrimination protocol. Furthermore, the designed setup allows for simulating fermionic particles with photons, thus assessing the role of exchange statistics in coherence generation and utilization. Our experiment proves that independent indistinguishable particles can offer a controllable resource of coherence and entanglement for quantum-enhanced metrology.

Identical particles | Quantum coherence | Quantum metrology

A quantum system can reside in coherent superpositions of states, which have a role in the interpretation of quantum mechanics (1–4), lead to nonclassicality (5, 6) and imply the intrinsic probabilistic nature of predictions in the quantum realm (7, 8). Besides this fundamental role, quantum coherence is also at the basis of quantum algorithms (9–14) and, from the modern information-theoretic perspective, constitutes a paradigmatic basis-dependent quantum resource (15–17), providing a quantifiable advantage in certain quantum information protocols.

For a single quantum particle, coherence emerges when the particle is found in a superposition of the computational basis of the Hilbert space. For multiparticle compound systems, the physics underlying the emergence of coherence is more prosperous and strictly connected to the nature of the particles, with fundamental differences for nonidentical and identical particles. A particularly intriguing observation is that the states of identical particle systems can manifest coherence even when *no* particle resides in superposition states, provided that the wavefunctions of the particles overlap (18–20). In general, a special contribution to quantum coherence arises thanks to the spatial indistinguishability of identical particles, which cannot exist for nonidentical (or distinguishable) particles (18). Recently, it has been found that the aptitude of spatial indistinguishability of identical particles can be exploited for entanglement generation (21), applicable even for spacelike-separated quanta (22) and against preparation and dynamical noises (23–25). The presence of entanglement is a signature that the bipartite system as a whole carries coherence even when the individual particles do not, the amount of this coherence being dependent on the degree of indistinguishability. We name this specific contribution to quantumness of compound systems as "indistinguishability-based coherence", as a difference with the more familiar "single-particle superposition-based coherence". Indistinguishability-based coherence qualifies in principle as an exploitable resource for quantum metrology

Significance Statement

Quantum coherence has a fundamentally different origin for nonidentical and identical particles, since for the latter a unique contribution exists due to indistinguishability. Here, we experimentally show how to exploit, in a controllable fashion, the contribution to quantum coherence stemming from spatial indistinguishability. Our experiment also directly proves, on the same footing, the different role of particle statistics (bosons or fermions) in supplying coherence-enabled advantage for quantum metrology. Ultimately, our results provide insights towards viable quantum-enhanced technologies based on tunable indistinguishability of identical building blocks.

R.L.F. proposed the experimental study. K.S. designed the experiment. K.S. performed the experiment with the assistance from Z.-H.L., Y.W. and Z.-Y.H.; A.C. derived the theoretical results with support from L.L., A.W., G.A and G.C.. R.L.F. supervised the theoretical part of the project. J.-S.X., C.-F.L. and G.-C.G. supervised the experimental parts of the project. All authors discussed the results and contributed to the writing of the manuscript.

The authors declare that they have no competing interests.

[1]K.S. and Z.-H.L. contributed equally to this work.

[2]To whom correspondence should be addressed. E-mail: jsxu@ustc.edu.cn (J.-S.X.), cfli@ustc.edu.cn (C.-F.L.), rosario.lofranco@unipa.it (R.L.F.)

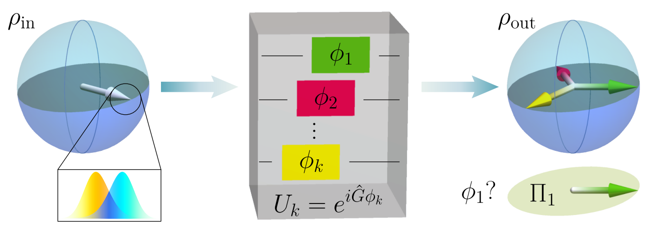

Fig. 1. Illustration of the indistinguishability-activated phase discrimination task. A resource state $\rho_{\rm in}$ that contains coherence on a computational basis is distilled from spatial indistinguishability. The state then enters a black box which implements a phase unitary $\hat{U}_k = e^{i\hat{G}\phi_k}, k \in \{1,\ldots,n\}$ on $\rho_{\rm in}$. The goal is to determine the ϕ_k actually applied through the output state $\rho_{\rm out}$: indistinguishability-based coherence provides operational advantage to the task.

(18). However, it requires sophisticated control techniques to be harnessed, especially in view of its nonlocal nature. Moreover, a crucial property of identical particles is the exchange statistics, while its experimental study requiring operating both bosons and fermions in the same setup is generally challenging.

In this work, we investigate the operational contribution of quantum coherence stemming from the spatial indistinguishability of identical particles. The main aim of our experiment is to prove that elementary states of two independent spatially-indistinguishable particles can give rise to exploitable quantum coherence, with a measurable effect due to particle statistics. By utilizing our recently developed photonic architecture capable of tuning the indistinguishability of two uncorrelated photons (26), we observe the direct connection between the degree of indistinguishability and the amount of generated coherence, and show that indistinguishability-based coherence can be concurrent with single-particle superposition-based coherence. In particular, we demonstrate its operational implications, namely, providing a quantifiable advantage in a phase discrimination task (27, 28), as depicted in Fig. 1. Furthermore, we design a setup capable of testing the impact of particle statistics in coherence production and phase discrimination for both bosons and fermions; this is accomplished by compensating for the exchange phase during state preparation, simulating fermionic states with photons, which leads to statistics-dependent efficiency of the quantum task.

Results

Indistinguishability-based coherence. To introduce the idea of coherence activated by spatial indistinguishability (18), we start from a simple scenario where the wavefunctions of two identical particles with orthogonal pseudospins, $\downarrow$ and $\uparrow$ overlap at two spatially-separated sites, L and R. Omitting the unphysical labeling of identical particles thanks to the no-label formalism (29), the state is described as $|\Psi\rangle = |\psi\downarrow, \psi'\uparrow\rangle$, with $|\psi\rangle = l\,|\mathrm{L}\rangle + r\,|\mathrm{R}\rangle$ and $|\psi'\rangle = l'\,|\mathrm{L}\rangle + r'\,|\mathrm{R}\rangle$ denoting the spatial wavefunctions corresponding to the two pseudospins. We stress that the no-label formalism adopted here reveals very suited for our investigations requiring a tunable degree of spatial indistinguishability of identical particles. In the Materials and Methods section, we provide a more thorough discussion about the advantages of the no-label formalism in describing identical particle systems.

Let us use spatially localized operations and classical communication, i.e., the sLOCC-framework (21), to activate and exploit the operational coherence. Projecting onto the operational subspace $\mathcal{B} = \{|L\sigma, R\tau\rangle\,;\sigma,\tau =\downarrow,\uparrow\}$ yields the normalized conditional state (18)

$$|\Psi_{\mathrm{LR}}\rangle = \frac{1}{\mathcal{N}_{\mathrm{LR}}^{\Psi}}(lr'\,|\mathrm{L}\downarrow, \mathrm{R}\uparrow\rangle + \eta l'r\,|\mathrm{L}\uparrow, \mathrm{R}\downarrow\rangle), \qquad [1]$$

with $\mathcal{N}_{\mathrm{LR}}^{\Psi} = \sqrt{|lr'|^2 + |l'r|^2}$, and the exchange phase factor $\eta = 1(-1)$ originates from the bosonic (fermionic) nature of the indistinguishable particles. We see that, although each particle starts from an incoherent state (namely, $|\psi\downarrow\rangle$, $|\psi'\uparrow\rangle$) in the pseudospin computational basis, the final state $|\Psi_{\mathrm{LR}}\rangle$ overall resembles a coherent, nonlocally-encoded qubit state in the compound basis $\mathcal{B}$ under sLOCC. Also, considering that this coherence vanishes when the two particles are nonidentical thus individually addressable (18), the emergence of coherence in $|\Psi_{\mathrm{LR}}\rangle$ essentially hinges on the spatial indistinguishability of the identical particles, in strict analogy to the emergence of entanglement between pseudospins (21, 26, 30).

The coherence of the state of Eq. (1) is independent of the bosonic or fermionic nature of the particles because of the specific choice of the initial single-particle states. However, in general, particle statistics plays a role in determining the allowed spatial overlap properties of identical particles and is thus crucial for the coherence of the overall state of the system. Hence, we shall extend our experimental investigation to a state where these fundamental aspects can be observed. Taking again a scenario with two indistinguishable particles, one of the particles is now initialized with innate coherence in the pseudospin basis, i.e., the initial two-particle state reads $|\Psi'\rangle = |\psi\downarrow, \psi's'\rangle$, where $|s'\rangle = a\,|\uparrow\rangle + b\,|\downarrow\rangle$ with $|a|^2 + |b|^2 = 1$. Projecting onto $\mathcal{B}$ generates the three-level distributed state (18)

$$|\Phi_{\mathrm{LR}}\rangle = \frac{1}{\mathcal{N}_{\mathrm{LR}}^{\Phi}}(alr'\,|\mathrm{L}\downarrow, \mathrm{R}\uparrow\rangle + b(lr' + \eta l'r)\,|\mathrm{L}\downarrow, \mathrm{R}\downarrow\rangle + a\eta l'r\,|\mathrm{L}\uparrow, \mathrm{R}\downarrow\rangle), \qquad [2]$$

where $\mathcal{N}_{\mathrm{LR}}^{\Phi} = \sqrt{a^2(|lr'|^2 + |l'r|^2) + b^2|lr' + \eta l'r|^2}$. In this state, indistinguishability-based coherence coexists with single-particle superposition-based coherence, giving rise to an overall multilevel coherence in the operational basis $\mathcal{B}$.

A photonic coherence synthesizer. We prepare two-level and three-level indistinguishability-based coherence by utilizing the photonic configuration shown in Fig. 2. The

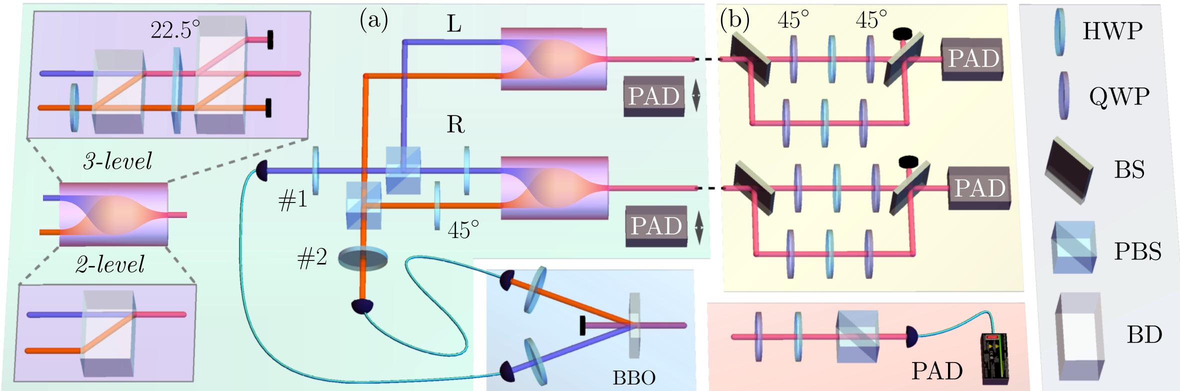

Fig. 2. Experimental configuration. (a) Preparation of coherent resource states by implementing sLOCC on indistinguishable particles. Photon pairs with orthogonal polarization states are prepared by pumping a β-barium borate (BBO) crystal. The two-photon wavefunctions are distributed in two spatial regions, with the indistinguishability tuned by the half-wave plates (HWPs) #1 and #2. The purple boxes represent the beam combiners are inserted to overlap the wavefunctions of two indistinguishable photons. The inset shows the detailed configuration of the beam combiner. For the activation of two-level coherence (lower subplot), a beam displacer (BD) combines the propagating paths of the two incoming photons; for the three-level case (upper subplot), an additional HWP initializes the polarization state of one of the photons, the horizontally- and vertically-polarized wavefunction amplitudes of the photon are then successively joined in the propagating path of the other photon with a pair of BDs and a HWP in between. (b) Discrimination of different phases. The Franson interferometer creates two phase channels with different configurations, which is adjusted by the HWP sandwiched between two quarter-wave plates (QWPs). The polarization analysis device (PAD) comprises a QWP, a HWP, a polarizing beam splitter (PBS) and a single-photon detector. BS: non-polarizing beam splitter.

correspondence between photon's polarization and pseudospin reads $|H\rangle \sim |{\uparrow}\rangle$, $|V\rangle \sim |{\downarrow}\rangle$, with $|H\rangle$ and $|V\rangle$ identifying horizontal and vertical polarization, respectively. As shown in Fig. 2(a), frequency-degenerate photon pairs are generated by pumping a beamlike type-II β-barium borate (BBO) crystal via spontaneous parametric down-conversion (31), and sent to the main setup via two single-mode fibers, respectively. The two-photon initial state $|H\rangle \otimes |V\rangle$ is uncorrelated, and two half-wave plates (HWPs, #1 and #2) with their orientation set at 22.5° and $\theta/2$, respectively, are utilized to adjust their polarizations. Each of the two initially uncorrelated photons then passes through a polarizing beam splitter (PBS), which distributes their spatial wavefunctions between two remote sites, L and R, according to the polarization state. Next, additional HWPs at 45° are inserted in different paths to revert the photons' initial polarization.

The activation of functional quantum coherence from spatial indistinguishability of two photons is achieved by a *beam combiner* comprised of a set of beam displacer (BD) arrays. A beam displacer is a birefringent calcite crystal with a suitably cut optical axis leading the vertical and horizontal polarizations of photons to separate parallelly. For the preparation of the two-level state $|\Psi_{\rm LR}\rangle$, the beam combiner is comprised of the setup already employed in the demonstration of polarization-entanglement activation by spatial indistinguishability (26) (see the lower inset of Fig. 2(a)). Explicitly, a BD on each site combines the propagating directions of the two photons, in which the horizontally polarized photon is displaced while the vertically polarized photon does not change the propagating direction. At this point, the spatial wavefunctions of the two photons become overlapped, allowing for preparing the state $|\Psi_{\rm LR}\rangle$ via sLOCC. A pair of polarization analysis devices (PADs) can be inserted after the beam combinerto cast polarization measurement, and the coincidence photon counting process realizes the desired projection onto the distributed basis $\mathcal{B}$. To prepare the three-level state $|\Phi_{\rm LR}\rangle$, an elaborate beam combiner setup is appended on each site, L and R (see the upper inset of Fig. 2(a)). We defer the detailed description and setup mechanism to the Materials and Methods section.

As a first observation, we want to prove the direct quantitative connection between produced coherence and spatial indistinguishability of photons, in analogy to what has been done for the entanglement (26). In fact, in the present experimental study, the resource of interest is quantum coherence; such a preliminary analysis is essential in view of its controllable exploitation for the specific quantum metrology protocol. This analysis is performed for the two-level state $|\Psi_{\rm LR}\rangle$ resulting from the original elementary state $|\Psi\rangle$. Various methods have been proposed to quantify coherence (27, 32–35). Here, we adopt the l_1 norm of the density matrix ρ, that is $C_{l_1}(\rho) = \sum_{i\neq j} |\rho_{ij}|$ (32). The system is prepared in $|\Psi_{\rm LR}(\theta)\rangle = \cos\theta\,|{\rm L}\uparrow, {\rm R}\downarrow\rangle + \sin\theta\,|{\rm L}\downarrow, {\rm R}\uparrow\rangle$, and its measure of coherence in the basis $\mathcal{B}$ is $C_{l_1}(\Psi_{\rm LR}) = |\sin 2\theta\,|$. The coherence completely stems from the indistinguishability of the photons, as it vanishes at the limit $\theta = k\pi/2$ (k integer number), i.e., when the two photons are distinguishable.

To quantify the spatial indistinguishability of the two photons we use the entropic measure (23) $\mathcal{I} = -\sum_{i=1}^{2} p_{\rm LR}^{(i)} \log p_{\rm LR}^{(i)}$, where $p_{\rm LR}^{(1)} = |lr'/\mathcal{N}_{\rm LR}^{\Phi}|^2$ ($p_{\rm LR}^{(2)} = |l'r/\mathcal{N}_{\rm LR}^{\Phi}|^2$) refers to the probability of finding the photon from ψ and ψ' (ψ' and ψ) ending at L and R, respectively. For our setup, one has $\mathcal{I} = -\cos^2\theta \log(\cos^2\theta) - \sin^2\theta \log(\sin^2\theta)$. The experimental result for the measurement of coherence versus indistinguishability is plotted in Fig. 3(a), clearly revealing the monotonic dependence in accord with theoretical predictions. The inset shows the result of quantum state tomography at $\theta=\pi/4$, which has a fidelity of 0.988 to the maximally coherent state. Hereafter, the error bars represent the 1σ standard deviation of data points, which is deduced by assuming a Poisson distribution for counting statistics, and resampling over the collected data (36). The Poisson-type uncertainty propagation method is widely adopted in the error estimation of various photonic experimental contexts, e.g., the test of non-local realism (37), boson sampling (38), integrated photonics (39), and fiber-based scenarios (40).

Phase discrimination. Having generated tunable coherence using sLOCC, we apply it in the phase discrimination task to demonstrate the operational advantage due to indistinguishability and the role of particle statistics. The formal definition of phase discrimination task is as follows: a phase unitary among n possible choices $U_k = e^{i\hat{G}\phi_k}, k \in \{1,\dots,n\}$ is randomly applied on an initial state $\rho_{\rm in}$ with a probability of p_k, where the generator of the transformation $\hat{G} = \sum_{\sigma\tau=\uparrow,\downarrow}\omega_{\sigma\tau}\left|{\rm L}\sigma,{\rm R}\tau\right\rangle\left\langle{\rm L}\sigma,{\rm R}\tau\right|$ is diagonal on the computational basis ($\omega_{\sigma\tau}$ are arbitrary coefficients) and $\sum_{k=1}^{n}p_k=1$. We shall identify the ϕ_k that is actually applied with maximal confidence from the output state $\rho_{\rm out}$, by casting positive operator-valued measurements (POVMs). Here, we focus on the $n=2$ scenario with $\phi_1=0$, $\phi_2=\phi$, and solve the task using the experimentally feasible minimum-error discrimination (41, 42).

We first investigate phase discrimination with the two-level state and, without loss of generality, choose the generator $\hat{G} = \left|{\rm L}\uparrow,{\rm R}\downarrow\right\rangle\left\langle{\rm L}\uparrow,{\rm R}\downarrow\right|$ (obtained fixing $\omega_{\uparrow\downarrow}=1$ and $\omega_{\uparrow\uparrow}=\omega_{\downarrow\uparrow}=\omega_{\downarrow\downarrow}=0$). Consequently, the output states after being affected by U_k read

$$\left|\Psi^k\right\rangle = \frac{1}{\mathcal{N}_{\rm LR}^{\Psi}}\left(lr'\left|{\rm L}\downarrow,{\rm R}\uparrow\right\rangle + \eta l'r e^{i(k-1)\phi}\left|{\rm L}\uparrow,{\rm R}\downarrow\right\rangle\right), \quad [3]$$

and they are discriminated by a POVM (a von Neumann projective measurement in this case) comprising two projectors $\mathbf{\Pi}=\{\hat{\Pi}_1,\hat{\Pi}_2\}$: when $\hat{\Pi}_k$ clicks, the phase is identified as ϕ_k. By this definition, the chance of making an error is $P_{\rm err} = p_1\langle\Psi^1|\hat{\Pi}_2|\Psi^1\rangle + p_2\langle\Psi^2|\hat{\Pi}_1|\Psi^2\rangle$, and is lower bounded by the Helstrom-Holevo bound (43, 44), namely, $P_{\rm err} \geqslant \frac{1}{2}\left(1-\sqrt{1-4p_1p_2\left|\langle\Psi^1|\Psi^2\rangle\right|^2}\right)$. For a two-level coherent state, it is straightforward to identify the measurement projectors $\hat{\Pi}_1$ and $\hat{\Pi}_2$ (18).

The phase discrimination game is experimentally realized using the setup of Fig. 2(b). The photons in the state $|\Psi_{\rm LR}\rangle$ on the site R are sent into an unbalanced Mach-Zehnder interferometer (UMZI), while the photons on the site L are directly detected. We put a HWP between two QWPs fixed at 45° to build a phase gate, and place one phase gate into each of the arms after a non-polarization beam splitter (BS). In the short arm of UMZI, the choice of the phase gate angle leaves the state $|\Psi_{\rm LR}\rangle$ unchanged, while in the long arm, a relative phase ϕ between $|{\rm L}\downarrow,\ {\rm R}\uparrow\rangle$ and $|{\rm L}\uparrow,\ {\rm R}\downarrow\rangle$ is imported. A movable shutter (not shown) is placed in one of the arms to adjust the parameters p_1 and p_2. After the UMZI, the photons are projected on the desired state. Since $|\Psi_{\rm LR}\rangle$ is a two-level coherent state, the measurement projectors $\hat{\Pi}_1$ and $\hat{\Pi}_2$ defined in the basis $\{|{\rm L}\downarrow,\ {\rm R}\uparrow\rangle,\ |{\rm L}\uparrow,\ {\rm R}\downarrow\rangle\}$ are realized in the corresponding subspace from the product (single-particle) state measurement. This procedure is as follows. On the site L (R), the polarization projector is $\hat{O}_{\rm L} = |\chi\rangle\langle\chi|$ with $|\chi\rangle = \alpha|\uparrow\rangle + \beta|\downarrow\rangle$ ($\hat{O}'_{\rm R} = |\chi'\rangle\langle\chi'|$ with $|\chi'\rangle = \alpha'|\uparrow\rangle + \beta'|\downarrow\rangle$). The product projector is thus $\hat{O}_{\rm L}\otimes\hat{O}'_{\rm R}$, leading to the two-photon projector $|\Psi_{\alpha\beta}\rangle\langle\Psi_{\alpha\beta}|$ with $|\Psi_{\alpha\beta}\rangle = \alpha\beta'|{\rm L}\uparrow,\ {\rm R}\downarrow\rangle + \beta\alpha'|{\rm L}\downarrow,\ {\rm R}\uparrow\rangle$ in the subspace of interest $\{|{\rm L}\downarrow,\ {\rm R}\uparrow\rangle,\ |{\rm L}\uparrow,\ {\rm R}\downarrow\rangle\}$. Thanks to the final PAD unit of the setup of Fig. 2(b), the parameters $\{\alpha,\ \beta,\ \alpha',\ \beta'\}$ can be adjusted to perform the desired projective measurements $\hat{\Pi}_1$, $\hat{\Pi}_2$ and eventually obtain the error probability of discrimination $P_{\rm err}$.

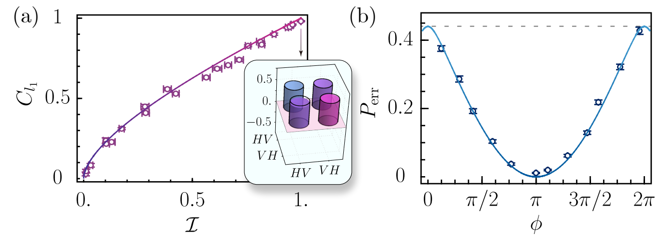

Fig. 3. Experimental result for the two-level state $|\Psi_{\rm LR}\rangle$. The points and curves represent experimental results theoretical predictions, respectively. (a) Quantification of coherence C_{l_1} versus the two-photon indistinguishability $\mathcal{I}$. The inset shows the real part of the density matrix for the input state $|\Psi_{\rm LR}(\pi/4)\rangle$ deduced by quantum state tomography. The basis correspondences read $|HV\rangle \sim |{\rm L}\uparrow,\ {\rm R}\downarrow\rangle$, $|VH\rangle \sim |{\rm L}\downarrow,\ {\rm R}\uparrow\rangle$. (b) The error probability $P_{\rm err}$ of phase discrimination versus the phase parameter ϕ, with $\theta=\pi/4$ to give maximal coherence and $p_1=0.44$. The dashed line shows the Helstrom-Holevo bound without coherence.

We directly measure the error probability of phase discrimination for various ϕ at $p_1=0.44$ by employing the maximally coherent state $|\Psi_{\rm LR}(\pi/4)\rangle$ and optimizing over the measurement settings of $\hat{\Pi}_1$ and $\hat{\Pi}_2$. The experimental result, matching well with the theoretical prediction,

$$P_{\rm err} = \frac{1}{2}\left(1-\sqrt{1-2p_1(1-p_1)(1+\cos\phi)}\right), \quad [4]$$

is shown in Fig. 3(b). Note that without coherence, the best strategy of phase discrimination is to constantly guess the phase with greater probability, yielding $\bar{P}_{\rm err}=p_1$ (top dashed line). The reduced $P_{\rm err}$ thus unravels the almost ubiquitous advantage of indistinguishability-based coherence.

Emulating different particle statistics. The symmetric form of Eq. (3) prevents the exchange phase factor η from affecting the outcome of $|\Psi_{\rm LR}\rangle$-based phase discrimination task. However, when the three-level coherent state, $|\Phi_{\rm LR}\rangle$, is utilized in the same task, the intrinsic statistics of the indistinguishable particles renders the situation more complicated. The bosonic nature of the photons guarantees zero exchange phase, a property both from the quantum axiom and experimentally testable (45). Hence, the quantum states prepared in our setup naturally has $\eta = +1$. Throughout this section, we fix one of the photons at maximal superposition state $|s'\rangle = (|\uparrow\rangle + |\downarrow\rangle)/\sqrt{2}$, i.e., set $a = b$ for simplicity which is implemented with setting both HWPs, placed before the first BD in the three-level setup, to be 22.5°. Choosing the mixing parameters as $l = l' = r = r'$ ($l' = r = 0$) maximizes (destroys) the bosonic indistinguishability; this is experimentally achieved by setting the orientation of both HWPs #1 and #2 be 22.5° ($\pi/4$).

On the other hand, photonic simulations of the dynamics of fermionic (46–48) and non-Abelian anyonic systems (49) may provide additional insights for the exotic physics therein. From the observation that η in Eq. (2) can be absorbed into l', a viable investigation of fermionic systems with $\eta = -1$ can be achieved using our setup: by setting $\theta = -\pi/4$, we invert the sign of l' to simulate indistinguishability-activated coherence of fermionic particles. Note that the previous simulations of fermionic or anyonic behavior via photons inevitably rely on either a highly entangled singlet state as the input state or non-local mathematical correspondences like Jordan–Wigner transformation to supply the anti-symmetric exchange behavior. Both methods limit the scalability of simulation and scramble some topological order. In stark contrast, the applicability of our simulation method, which directly emulates the exchange properties of identical particles by harnessing the spatial indistinguishability of photons, is not limited by the above hurdles.

The prepared states emulating bosonic, distinguishable and fermionic particles are characterized via quantum state tomography, and the results are presented in Fig. 4(a). The three cases have fidelity of 98.4%, 97.5%, and 97.7%, respectively. For the bosonic case, the outcome authenticates the presence of coherence between all three vectors of the computational basis shown in Eq. (2). For the distinguishable case ($l' = r = 0$), the coherence is in contrast solely inherited from one of the particles, and localized on the site R. For the fermionic case, the resulted state in Eq. (2) interestingly becomes a two-level state, $|\Psi_{\rm LR}(\pi/4)\rangle$, since the destructive interference almost completely eliminates the amplitude on the basis $|{\rm L}\downarrow, {\rm R}\downarrow\rangle$. And this matches the prediction of Pauli exclusion principle where the pseudospins of two particles are opposite. In our experiment, the exchange phase is obtained via the tomographic results as $(0.988 \pm 0.016)\pi$ supporting a fermion-like exchange behavior of the photons due to the compensation. Note that a minus sign appears in the coefficient of the $|{\rm L}\downarrow, {\rm R}\uparrow\rangle$ terms, which is attributed to the π-phase acquired by the photons upon reflected by PBS.

We are now in the position to investigate the role of particle statistics in the phase discrimination task. The corresponding operations U_k are again realized using the phase gates within the UMZI, yielding two output states $|\Phi^k\rangle$ (18) written as

$$|\Phi^k\rangle = (a(lr'e^{i\omega_{\downarrow\uparrow}\phi_k}|L\downarrow, R\uparrow\rangle + \eta l'r e^{i\omega_{\uparrow\downarrow}\phi_k}|L\uparrow, R\downarrow\rangle) + b(lr' + \eta l'r)e^{i\omega_{\downarrow\downarrow}\phi_k}|L\downarrow, R\downarrow\rangle)/\mathcal{N}^{\Phi}_{LR}. \quad [5]$$

Here, we set $\omega_{\downarrow\uparrow} = 1$, $\omega_{\uparrow\downarrow} = 2$ and $\omega_{\downarrow\downarrow} = 3$ in the generator $\hat{G}$. Unlike the two-level situation, in this three-level coherent case we need to place an UMZI on each site L and R. The UMZI has a path difference equivalent to 2.7ns between the long and short paths, and the coincidence interval is set at 0.8ns. The quantum states affected by the two phase operations in the UMZIs are registered separately (50, 51). We adjust the electric delay of the coincidence module to pick out the events that the two photons had taken the long/short and short/long paths, which correspond to the state after being affected by U_1 and U_2, respectively. Moreover, for the measurement of the three-level system, to minimize the error probability of discrimination $P_{\rm err}$, three projectors $\hat{\Pi}_1$, $\hat{\Pi}_2$ and $\hat{\Pi}_3$ are required where $\Sigma_i^3 \hat{\Pi}_i = I$ and ${\rm Tr}[\hat{\Pi}_3 |\Phi^1_{\rm LR}\rangle\langle\Phi^1_{\rm LR}|] = {\rm Tr}[\hat{\Pi}_3 |\Phi^2_{\rm LR}\rangle\langle\Phi^2_{\rm LR}|] = 0$. The projectors $\hat{\Pi}_i$ ($i = 1,\ 2,\ 3$) consist of three linearly independent basis vectors $\mathcal{B}' = \{|{\rm L}\uparrow, {\rm R}\downarrow\rangle, |{\rm L}\downarrow, {\rm R}\uparrow\rangle, |{\rm L}\downarrow, {\rm R}\downarrow\rangle\}$ (see details in the Materials and Methods section). Similarly to the method used above for the two-level state, these three projectors are also extracted from the subspace of the product projectors on the two sites L and R and implemented by the PAD unit of the setup.

Fig. 4(b) reports the measured error probabilities for

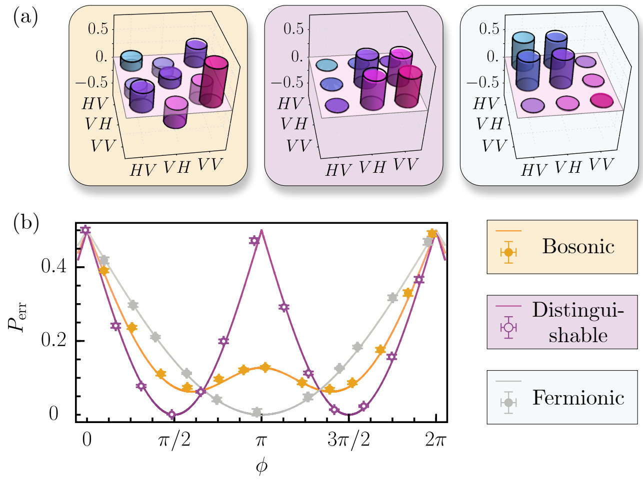

Fig. 4. Experimental result for three-level state $|\Phi_{\rm LR}\rangle$. (a) The real part of the density matrix for the input states $|\Phi_{\rm LR}\rangle$ of bosonic, distinguishable ($l' = r = 0$) and fermionic particles (simulated), deduced by quantum state tomography, with $\theta = \pm\pi/4$ to give maximal coherence. The magnitude of the imaginary part of the density matrices are smaller than 0.07. The basis correspondences read $|HV\rangle \sim |{\rm L}\uparrow, {\rm R}\downarrow\rangle$, $|VH\rangle \sim |{\rm L}\downarrow, {\rm R}\uparrow\rangle$, and $|VV\rangle \sim |{\rm L}\downarrow, {\rm R}\downarrow\rangle$. (b) The error probability $P_{\rm err}$ of phase discrimination versus ϕ for bosonic, distinguishable and simulated fermionic particles with $p_1 = 0.50$. The experimental results are presented by dots with error bars in different appearances. The solid curves are the theoretical predictions with $\omega_{\downarrow\uparrow} = 1$, $\omega_{\uparrow\downarrow} = 2$ and $\omega_{\downarrow\downarrow} = 3$.

phase discrimination with the three-level states. A clear discrepancy between the credibility of phase discrimination using different kinds of particles can be observed. Particularly, both types of indistinguishable particles provide advantage over distinguishable ones within the range of $\phi \in (\frac{2\pi}{3}, \frac{4\pi}{3})$, but fermions further outperform bosons by a difference in P_{err} of 0.119 at $\phi = \pi$. This can be intuitively interpreted by recalling that the exchange interaction of fermions prevent them from occupying the same state, so the wavefunction amplitude disperses between different states and produces large amount of coherence. In contrast, bosons tend to bunch on a single state, so the applicable coherence is reduced. The experimental result for the fermionic three-level case, as shown in Fig. 4(b), appears similar but not identical to a reported two-level case given in the earlier text (see Fig. 3(b)). In the experimental configuration here, the wavefunction amplitude of $|\mathrm{L}\downarrow, \mathrm{R}\downarrow\rangle$ vanishes due to the destructive interference when two trajectories of indistinguishable particles coalesce on the BD. Also, the two discrimination games are subject to slightly different subchannel probabilities p_1.

Discussion

Coherence activated from spatial indistinguishability is a fundamental contribution to the quantumness of multiparticle composite systems intimately related to the presence of identical particles (subsystems). It cannot exist between different types of quanta, that is, in systems made of nonidentical (or distinguishable) particles. Due to its intrinsic nonlocal trait, in order to apply the indistinguishability-based coherence in quantum information tasks, transformations and measurements on the resource state must admit direct product decomposition into local operations, which are achieved by sLOCC. We note that in the case of two identical particles, Schmidt decomposition recovers our capability to perform all possible measurements (52). Therefore, applying indistinguishability-based coherence between three or more quanta will be an open research route.

In this paper, we have experimentally investigated indistinguishability-based coherence, demonstrating its operational usefulness in a quantum metrology protocol. Our photonic architecture is capable of tuning the degree of spatial indistinguishability of two uncorrelated photons, and adjusting the interplay between indistinguishability-based coherence and single-particle superposition-based coherence to synthesize hybrid, multilevel coherence from two non-orthogonal pseudospins. This has allowed us to prepare via sLOCC various types of resource states by devising and implementing a beam combiner, and characterize the operational coherence via the phase discrimination task. Our results highlight, in a comprehensive fashion, the fundamental and practical aspects of controllable indistinguishability of identical building blocks for quantum-enhanced technologies.

A particularly interesting feature of our setup is that it has been devised in such a way that both bosonic and fermionic statistics can occur in the resource states, thus enabling the possibility to directly observe how the nature of the employed particles affects the efficiency of the quantum task. The present experiment also shows that, within the usual first quantization approach with fictitious labels to describe identical particle states, the superpositions of a two-particle state and its permuted version enforced by the symmetrization postulate gives rise to true, physical entanglement (e.g., $|\psi\downarrow, \psi'\uparrow\rangle \leftrightarrow \frac{1}{\sqrt{2}}(|\psi\downarrow\rangle_A \otimes |\psi'\uparrow\rangle_B + \eta\, |\psi'\uparrow\rangle_A \otimes |\psi\downarrow\rangle_B)$, where fictitious labels A and B have been adopted). This result can be seen as a confirmation of what one can deduce from a recent experiment to directly measure the statistics exchange phase of photons (45, 53), where a quantum interference between a reference state and its physically exchanged version is created. In our experiment, such an entanglement, due to the enabled quantum coherence, is entirely contained in the elementary state of two independent spatially-indistinguishable photons expressed in the no-label formalism, with the particle statistics imprint emerging in the final state after the sLOCC measurement. As an outlook, it would be interesting to develop a similar experiment with actual fermions. Platforms with devices realizing linear optics operations with fermions, such as electrons, would be the best candidates. To this purpose, one may use quantum dots as sources of single electrons that can be emitted on demand (54), initialized in given spin states (55), and sent to quantum point contacts operating like electronic beam splitters (56, 57). Atomic circuits may also be employed to control single electrons (58). Our experiment thus paves the way to suitably exploit these different platforms to investigate indistinguishability-enabled quantum coherence with real fermions.

We finally remark that the observed phenomena in our experiment do not only follow a mapping of a fermionic state into a photonic system. Indeed, they recover fundamental traits of the original fermionic system. For example, we have observed that the π-exchange (fermionic) phase from optical compensation causes the photonic wavefunction on the symmetric state to vanish. This observation is in strict analogy to the Pauli exclusion principle found for real fermions forbidding multiple occupations of the same state: both these behaviors originate from the destructive interference due to the exchange of identical fermionic particles in the superposed two-particle states. Therefore, our work also constitutes an eligible quantum simulation of different kinds of identical particles and may shed further light on the characterization of this kind of compound systems, including anyons. Notably, the investigation of anyonic braiding may facilitate fault-tolerant quantum computation and information processing protocols (49, 59). To this end, our setup provides a pathway to address this problem naturally and intuitively. These studies constitute one of the main prospects motivated by the present work and will be investigated in the near future.

Materials and Methods

In this section, we start with a comprehensive discussion of the merit of the no-label formalism in the description of identical particles. We then present the detailed procedure for generating multilevel coherence via particle indistinguishability and applying it in a quantum metrological task.

Practical merits of the no-label formalism. The no-label formalism describing identical particles is a powerful tool suitable for various practical scenarios. Its main features are as follows: (i) it avoids fictitious labels which may complicate the analysis, (ii) directly encompasses bosons and fermions on the same footing; (iii) allows for the natural introduction of a continuous degree of spatial indistinguishability of experimentally-friendly use (23); (iv) permits to access physical entanglement by sLOCC (21, 29).

By virtue of the no-label formalism in our analysis, the difference between the particle (statistics) exchange behaviors can be completely absorbed in a different exchange phase of the final state obtained by sLOCC. Therefore, the no-label formalism can facilitate the photonic simulation of fermionic exchange by compensation of the exchange phase. Moreover, its equivalence with the standard formalism on the mathematical level guarantees that, when we map the bosonic state into the fermionic Hilbert space, the result will remain unchanged even from the viewpoint of the standard formalism (i.e., from both first quantization approach with fictitious labels and second quantization approach, see also: References (19, 60–62). For all these reasons, the no-label formalism has been largely adopted during recent years for both theoretical and experimental analyses (26, 30, 63, 64).

Generation of multilevel coherence. Here, we describe the procedure of generating the three-level, hybrid (indistinguishability- and superposition-based) coherence with beam combiner. The initial state $|\Psi'\rangle = |\psi\downarrow, \psi' s'\rangle = |\psi\downarrow, \psi'(a\uparrow + b\downarrow)\rangle$ is realized by placing another HWP before the first BD on each site, L and R, to modify the pseudospin of $|\psi'\rangle$ from $|\uparrow\rangle$ to $a|\uparrow\rangle + b|\downarrow\rangle$. This is followed further by a σ_x-compensation causing the ψ' component to evolve to $b|\uparrow\rangle + a|\downarrow\rangle$; the effect of the compensation is also absorbed into the HWP. Inside the beam combiner, two BDs sandwiching a HWP oriented set at 22.5° at each site form a Mach-Zehnder interferometer. After the first BD in the interferometer, the photonic wavefunction corresponding to the first term of $b|\uparrow\rangle + a|\downarrow\rangle$, i.e. $b|\uparrow\rangle$, is displaced to the path of the other photon whose pseudospin is $|\downarrow\rangle$, and the remaining part $a|\downarrow\rangle$ passes directly. At this stage, the HWP fixed at 22.5° implements a Hadamard transformation on the spin states to erase the original path information of the two photons. The remaining part on the lower path now reads $a(|\psi'\uparrow\rangle + |\psi'\downarrow\rangle)/\sqrt{2}$, and the second BD merges its first term, $a|\psi'\uparrow\rangle/\sqrt{2}$, to the middle path which contains $|\psi\downarrow, b\psi'\downarrow\rangle/\sqrt{2}$. As the result, for the three output paths of the interferometer, the wavefunction of the upper one reads $|\psi\uparrow, b\psi'\uparrow\rangle/\sqrt{2}$, the middle path consists of the wavefunction $|\psi\downarrow, \psi'(a\uparrow + b\downarrow)/\sqrt{2}$, while the remaining part, $a/\sqrt{2}\,|\psi'\downarrow\rangle$, locates in the bottom path. Thus, we only need to extract photons in the middle path, in which $|\downarrow\rangle$ and $a|\uparrow\rangle + b|\downarrow\rangle$ are combined together, and discard photons located on the other two paths—these photons do not contribute to the final counting events. Following the same measurement method introduced above, the three-level state $|\Phi_{\mathrm{LR}}\rangle$ underpinning the system is finally activated.

Phase discrimination with three-level system. Comparing with the two-level case, some subtlety underlies the measurement of the three-level system: first, because Eq. (2) is spanned by three linearly independent basis vectors $\mathcal{B}' = \{|\mathrm{L}\uparrow, \mathrm{R}\downarrow\rangle, |\mathrm{L}\downarrow, \mathrm{R}\uparrow\rangle, |\mathrm{L}\downarrow, \mathrm{R}\downarrow\rangle\}$, a POVM consisting of only two rank-1 projectors cannot satisfy the requirement of completeness. As such, even the discrimination of two phases will require additional projectors. Second, the projectors that minimize the probability of committing errors are generally entangled and thus not directly viable. To resolve these issues, we construct two auxiliary projectors, orthogonal to both of the states $|\Phi^k\rangle$, to construct a POVM $\mathbf{\Pi} = \{\hat{\Pi}_1, \hat{\Pi}_2, \hat{\Pi}_3, \hat{\Pi}_4\}$ in the direct sum dilated 4-dimensional space $\mathcal{B}$, so that every element of the POVM admits the product expansion $\Pi_k = |\mathrm{L}s, \mathrm{R}s'\rangle\langle \mathrm{L}s, \mathrm{R}s'|$, with s and s' being the localized pseudospin states, and the POVM recovers the probability distribution on $\mathcal{B}'$. Any experimental trial that eventuates in the detection on the auxiliary projectors is counted as an incorrect discrimination, regardless of the actual phase applied.

ACKNOWLEDGMENTS. This work was supported by National Key Research and Development Program of China (Grants No. 2017YFA0304100), the National Natural Science Foundation of China (Grants Nos. 61725504, U19A2075, 61805227, 61975195, 11774335, and 11821404), Key Research Program of Frontier Sciences, CAS (Grant No. QYZDY-SSW-SLH003), Science Foundation of the CAS (Grant No. ZDRW-XH-2019-1), the Fundamental Research Funds for the Central Universities (Grant No. WK2470000026, No. WK2030380017), Anhui Initiative in Quantum Information Technologies (Grants No. AHY020100, and No. AHY060300). L.L. acknowledges support from the Alexander von Humboldt Foundation.

1. E Schrödinger, Die gegenwärtige situation in der quantenmechanik. *Naturwissenschaften* **23**, 823–828 (1935).
2. EP Wigner, Remarks on the mind-body question in *Philosophical reflections and syntheses.* (Springer), pp. 247–260 (1995).
3. D Frauchiger, R Renner, Quantum theory cannot consistently describe the use of itself. *Nat. Commun.* **9**, 3711 (2018).
4. KW Bong, et al., A strong no-go theorem on the wigner's friend paradox. *Nat. Phys.* **16**, 1199–1205 (2020).
5. AM Gleason, Measures on the closed subspaces of a hilbert space. *J. Math. Mech.* **6**, 885–893 (1957).
6. S Kochen, EP Specker, The problem of hidden variables in quantum mechanics. *J. Math. Mech.* **17**, 59–87 (1967).
7. MN Bera, A Acín, M Kuś, MW Mitchell, M Lewenstein, Randomness in quantum mechanics: philosophy, physics and technology. *Rep. Prog. Phys.* **80**, 124001 (2017).
8. X Yuan, H Zhou, Z Cao, X Ma, Intrinsic randomness as a measure of quantum coherence. *Phys. Rev. A* **92**, 022124 (2015).
9. PW Shor, Algorithms for quantum computation: discrete logarithms and factoring in *Proceedings 35th annual symposium on foundations of computer science.* (Ieee), pp. 124–134 (1994).
10. E Martin-Lopez, et al., Experimental realization of Shor's quantum factoring algorithm using qubit recycling. *Nat. Photon.* **6**, 773–776 (2012).
11. R Cleve, A Ekert, C Macchiavello, M Mosca, Quantum algorithms revisited. *Proc. R. Soc. Lond. A* **454**, 339–354 (1998).
12. LM Procopio, et al., Experimental superposition of orders of quantum gates. *Nat. Commun.* **6**, 7913 (2015).
13. S Aaronson, A Arkhipov, The computational complexity of linear optics in *Proceedings of the forty-third annual ACM symposium on Theory of computing.* pp. 333–342 (2011).

14. F Arute, et al., Quantum supremacy using a programmable superconducting processor. *Nature* **574**, 505–510 (2019).
15. A Winter, D Yang, Operational resource theory of coherence. *Phys. Rev. Lett.* **116**, 120404 (2016).
16. A Streltsov, G Adesso, MB Plenio, Colloquium: Quantum coherence as a resource. *Rev. Mod. Phys.* **89**, 041003 (2017).
17. E Chitambar, G Gour, Quantum resource theories. *Rev. Mod. Phys.* **91**, 025001 (2019).
18. A Castellini, et al., Indistinguishability-enabled coherence for quantum metrology. *Phys. Rev. A* **100**, 012308 (2019).
19. S Chin, J Huh, Entanglement of identical particles and coherence in the first quantization language. *Phys. Rev. A* **99**, 052345 (2019).
20. J Sperling, A Perez-Leija, K Busch, IA Walmsley, Quantum coherences of indistinguishable particles. *Phys. Rev. A* **96**, 032334 (2017).
21. R Lo Franco, G Compagno, Indistinguishability of elementary systems as a resource for quantum information processing. *Phys. Rev. Lett.* **120**, 240403 (2018).
22. A Castellini, B Bellomo, G Compagno, R Lo Franco, Activating remote entanglement in a quantum network by local counting of identical particles. *Phys. Rev. A* **99**, 062322 (2019).
23. F Nosrati, A Castellini, G Compagno, R Lo Franco, Robust entanglement preparation against noise by controlling spatial indistinguishability. *npj Quantum Inf.* **6**, 1–7 (2020).
24. F Nosrati, A Castellini, G Compagno, R Lo Franco, Dynamics of spatially indistinguishable particles and quantum entanglement protection. *Phys. Rev. A* **102**, 062429 (2020).
25. A Perez-Leija, et al., Endurance of quantum coherence due to particle indistinguishability in noisy quantum networks. *npj Quant. Inf.* **4**, 45 (2018).
26. K Sun, et al., Experimental quantum entanglement and teleportation by tuning remote spatial indistinguishability of independent photons. *Opt. Lett.* **45**, 6410–6413 (2020).
27. C Napoli, et al., Robustness of coherence: an operational and observable measure of quantum coherence. *Phys. Rev. Lett.* **116**, 150502 (2016).
28. M Ringbauer, et al., Certification and quantification of multilevel quantum coherence. *Phys. Rev. X* **8**, 041007 (2018).
29. R Lo Franco, G Compagno, Quantum entanglement of identical particles by standard information-theoretic notions. *Sci. Rep.* **6**, 20603 (2016).
30. MR Barros, et al., Entangling bosons through particle indistinguishability and spatial overlap. *Opt. Express* **28**, 38083–38092 (2020).
31. S Takeuchi, Beamlike twin-photon generation by use of type II parametric downconversion. *Opt. Lett.* **26**, 843–845 (2001).
32. T Baumgratz, M Cramer, MB Plenio, Quantifying coherence. *Phys. Rev. Lett.* **113**, 140401 (2014).
33. M Piani, et al., Robustness of asymmetry and coherence of quantum states. *Phys. Rev. A* **93**, 042107 (2016).
34. I Marvian, RW Spekkens, How to quantify coherence: Distinguishing speakable and unspeakable notions. *Phys. Rev. A* **94**, 052324 (2016).
35. YT Wang, et al., Directly measuring the degree of quantum coherence using interference fringes. *Phys. Rev. Lett.* **118**, 020403 (2017).
36. JB Altepeter, ER Jeffrey, PG Kwiat, Photonic state tomography. *Adv. At. Mol. Opt. Phys.* **52**, 105–159 (2005).
37. S Gröblacher, et al., An experimental test of non-local realism. *Nature* **446**, 871–875 (2007).
38. JC Loredo, et al., Boson sampling with single-photon fock states from a bright solid-state source. *Phys. Rev. Lett.* **118**, 130503 (2017).
39. D Llewellyn, et al., Chip-to-chip quantum teleportation and multi-photon entanglement in silicon. *Nat. Phys.* **16**, 148–153 (2020).
40. S Wengerowsky, et al., Entanglement distribution over a 96-km-long submarine optical fiber. *Proc. Natl. Acad. Sci.* **116**, 6684–6688 (2019).
41. SM Barnett, S Croke, Quantum state discrimination. *Adv. Opt. Photonics* **1**, 238–278 (2009).
42. PJ Mosley, S Croke, IA Walmsley, SM Barnett, Experimental realization of maximum confidence quantum state discrimination for the extraction of quantum information. *Phys. Rev. Lett.* **97**, 193601 (2006).
43. CW Helstrom, Quantum detection and estimation theory. *J. Stat. Phys.* **1**, 231–252 (1969).
44. AS Holevo, Investigations in the general theory of statistical decisions. *Proc. Steklov Inst. Math.* **124**, 1–140 (1976).
45. K Tschernig, et al., Direct observation of the particle exchange phase of photons. *Nat. Photon.* (2021).
46. L Sansoni, et al., Two-particle bosonic-fermionic quantum walk via integrated photonics. *Phys. Rev. Lett.* **108**, 010502 (2012).
47. JCF Matthews, et al., Observing fermionic statistics with photons in arbitrary processes. *Sci. Rep.* **3**, 1539 (2013).
48. F De Nicola, et al., Quantum simulation of bosonic-fermionic noninteracting particles in disordered systems via a quantum walk. *Phys. Rev. A* **89**, 032322 (2014).
49. ZH Liu, et al., Topological contextuality and anyonic statistics of photonic-encoded parafermions. *PRX Quantum* **2**, 030323 (2021).
50. SM Barnett, E Riis, Experimental demonstration of polarization discrimination at the helstrom bound. *J. Mod. Opt.* **44**, 1061–1064 (1997).
51. M Mohseni, AM Steinberg, JA Bergou, Optical realization of optimal unambiguous discrimination for pure and mixed quantum states. *Phys. Rev. Lett.* **93**, 200403 (2004).
52. S Sciara, R Lo Franco, G Compagno, Universality of schmidt decomposition and particle identity. *Sci. Rep.* **7**, 44675 (2017).
53. R Lo Franco, Direct measurement of fundamental statistics phase of photons. *Nat. Photon., press* (2021).
54. G Fève, et al., An on-demand coherent single-electron source. *Science* **316**, 1169–1172 (2007).
55. D Press, TD Ladd, B Zhang, Y Yamamoto, Complete quantum control of a single quantum dot spin using ultrafast optical pulses. *Nature* **456**, 218–221 (2008).
56. C Bäuerle, et al., Coherent control of single electrons: a review of current progress. *Rep. Prog. Phys.* **81**, 056503 (2018).
57. E Bocquillon, et al., Coherence and indistinguishability of single electrons emitted by independent sources. *Science* **339**, 1054–1057 (2013).
58. M Rashidi, et al., Initiating and monitoring the evolution of single electrons within atom-defined structures. *Phys. Rev. Lett.* **121**, 166801 (2018).
59. HL Huang, et al., Emulating quantum teleportation of a Majorana zero mode qubit. *Phys. Rev. Lett.* **126**, 090502 (2021).
60. G Compagno, A Castellini, R Lo Franco, Dealing with indistinguishable particles and their entanglement. *Philos. Transactions Royal Soc. A: Math. Phys. Eng. Sci.* **376**, 20170317 (2018).
61. AC Lourenço, T Debarba, EI Duzzioni, Entanglement of indistinguishable particles: A comparative study. *Phys. Rev. A* **99**, 012341 (2019).
62. G Paul, S Das, A Banerji, Maximum violation of monogamy of entanglement for indistinguishable particles by measures that are monogamous for distinguishable particles. *Phys. Rev. A* **104**, L010402 (2021).
63. D Lee, et al., Entangling three identical particles via spatial overlap. (2021).
64. Y Wang, et al., Experimental remote entanglement distribution in a photonic quantum network through multinode indistinguishability. (2021).